

5. G. J. Lithgow et al., *J. Gerontol.* **49**, B270 (1994); G. J. Lithgow et al., *Proc. Natl. Acad. Sci. U.S.A.* **92**, 7540 (1995).
6. P. L. Larsen, *Proc. Natl. Acad. Sci. U.S.A.* **90**, 8905 (1993); J. R. Vanfleteren, *Biochem. J.* **292**, 605 (1993).
7. P. M. Service et al., *Physiol. Zool.* **58**, 380 (1985).
8. J. L. Graves et al., *ibid.* **65**, 268 (1992).
9. R. Arking et al., *Dev. Genet.* **12**, 362 (1991).
10. W. C. Orr and R. S. Sohal, *Science* **263**, 1128 (1994).
11. T. Parkes et al., *Nature Genet.* **19**, 171 (1998).
12. L. Cooley, R. Kelley, A. Spradling, *Science* **239**, 1121 (1988).
13. To generate P-element insertion lines, we crossed females carrying eight copies of P{lacW} (25) on a compound X chromosome (C(1)RM) with *ry Ki P{ry<sup>+</sup> Δ2-3}*, which carries the transposase. Female progeny were then crossed individually with *w<sup>1118</sup>*. New P-element insertions on autosomes were identified by red eye color in male progeny. In any cross that generated progeny having different degrees of red eye color, suggestive of multiple insertions, we chose a single female with lighter eye color and back-crossed it to *w<sup>1118</sup>* for several generations, until the color was homogeneous. Each insertion was mapped to a chromosome by the use of balancers, tested for homozygous viability and fertility, and established as an independent line. After its isolation, *mth* was extensively out-crossed before further characterization to avoid nonspecific effects of genetic background (26).
14. F. M. Ashton and A. S. Crafts, *Mode of Action of Insecticide* (Wiley Interscience, New York, 1973).
15. A. R. Heydari et al., *Experientia* **50**, 1092 (1994); J. C. Wheeler, E. T. Bieschke, J. Tower, *Proc. Natl. Acad. Sci. U.S.A.* **92**, 10408 (1995).
16. M. Tatar, A. A. Khazaeli, J. W. Curtsinger, *Nature* **390**, 30 (1997).
17. The *mth* genomic DNA was probed by the ampicillin resistance gene contained in the P-element construct used to generate mutant lines (25).
18. To excise the P-element, we crossed *mth* females with *ry Ki P{ry<sup>+</sup> Δ2-3}*. The male jump-starters were then crossed to *w;TM3/TM6*. Progeny with white eyes were made homozygous and lines established. Two alleles were homozygous lethal before the L2 larval stage and so were maintained over the third chromosome balancers, TM3 or TM6.
19. Genomic DNA adjacent to the P-element insertion site in *mth* was retrieved by plasmid rescue (27). Pst I and Eco RI digestion were used to clone upstream and downstream genomic fragments (Fig. 3A). Analysis of the upstream DNA sequence by Blast search (28) revealed two homologous sequences (clones LD08316 and GM02553) in the Berkeley *Drosophila* Genome Project (BDGP) database. The GM02553 clone, despite containing regions with 67% identity to the *mth* nucleotide sequence, had 17 gaps in the alignment, so it is not the same gene. In contrast, the 747-nucleotide partial sequence of LD08316 in the BDGP database displayed greater than 99% identity to the upstream sequence, without any gap. The calculated smallest sum probability of the Blast search was  $1.5 \times 10^{-137}$ , well within the range of identical sequences. The full sequence of LD08316 (1948 nucleotides) (Fig. 3B) also corresponded to the downstream genomic sequence of *mth*. We then used the cDNA as a probe to isolate *mth* genomic DNA from a P1-phagemid grid from Genome Systems. Three P1 plasmids (DS05332, DS03799, and DS06692) from the BDGP contained the genomic region of the *mth* gene. These P1 clones have a common contig, DS00539, which maps at 61C on the third chromosome (BDGP database). A corresponding 7.9-kb Eco RI fragment from DS06692 was subcloned into pBluescript vector and the full-length sequence determined.
20. S. F. Altschul et al., *Nucleic Acids Res.* **25**, 3389 (1997).
21. S. Henikoff and J. G. Henikoff, *Genomics* **19**, 97 (1994).
22. B. K. Kobilka et al., *Science* **240**, 1310 (1988); T. Kubo et al., *FEBS Lett.* **241**, 119 (1988); S. K. Wong, C. Slaughter, A. E. Ruoho, E. M. Ross, *J. Biol. Chem.* **263**, 7925 (1988); J. Ostrowski, M. A. Kjelsberg, M. G. Caron, R. J. Lefkowitz, *Annu. Rev. Pharmacol. Toxicol.* **32**, 167 (1992); E. S. Burstein, T. A. Spalding, M. R. Brann, *Biochemistry* **37**, 4052 (1998).
23. G. A. Walker, D. W. Walker, G. J. Lithgow, *Ann. N.Y. Acad. Sci.* **851**, 444 (1998).
24. S. Watson and S. Arkin, *The G-protein Linked Receptor Facts Book* (Academic Press, London, 1994); G. Vassart et al., *Ann. N.Y. Acad. Sci.* **766**, 23 (1995); T. P. Sakmar, *Prog. Nucleic Acid Res. Mol. Biol.* **59**, 1 (1998).
25. E. Bier et al., *Genes Dev.* **3**, 1273 (1989).
26. J. Tower, *Bioessays* **18**, 799 (1996).
27. B. A. Hamilton and K. Zinn, in *Methods in Cell Biology*, L. S. B. Goldstein and E. A. Fryberg, Eds. (Academic Press, San Diego, 1994), vol. 44, p. 81.
28. S. F. Altschul et al., *J. Mol. Biol.* **215**, 403 (1990).
29. J. Kyte and R. F. Doolittle, *ibid.* **157**, 105 (1982).
30. Supported by a Postdoctoral Research Fellowship from the John Douglas French Alzheimer Foundation (Y.-J.L.) and grants from the National Science Foundation (MCB9408718), the National Institutes of Health (EY09278 and AG12289), and the James G. Boswell Foundation (S.B.).

14 July 1998; accepted 25 September 1998

## Cardiovascular Failure in Mouse Embryos Deficient in VEGF Receptor-3

Daniel J. Dumont,\*† Lotta Jussila,\* Jussi Taipale,\*  
Athina Lymboussaki, Tuija Mustonen, Katri Pajusola,  
Martin Breitman,‡ Kari Alitalo§

Vascular endothelial growth factor (VEGF) is a key regulator of blood vessel development in embryos and angiogenesis in adult tissues. Unlike VEGF, the related VEGF-C stimulates the growth of lymphatic vessels through its specific lymphatic endothelial receptor VEGFR-3. Here it is shown that targeted inactivation of the gene encoding VEGFR-3 resulted in defective blood vessel development in early mouse embryos. Vasculogenesis and angiogenesis occurred, but large vessels became abnormally organized with defective lumens, leading to fluid accumulation in the pericardial cavity and cardiovascular failure at embryonic day 9.5. Thus, VEGFR-3 has an essential role in the development of the embryonic cardiovascular system before the emergence of the lymphatic vessels.

Disruption of VEGF or either of its two receptors VEGFR-1 (Flt-1) or VEGFR-2 (Flk-1) results in early embryonic death because of a failure of blood vessel development (1–4). The related placenta growth factor (PlGF) and VEGF-B signal through VEGFR-1 (5), whereas VEGF-C and VEGF-D can use both VEGFR-3 and VEGFR-2 for signaling (6–8). The expression of VEGFR-3 (Flt4) starts during mouse embryonic day (E) 8 in developing blood vessels but becomes largely restricted to the lymphatic vessels after their formation (9).

To analyze the biological role of VEGFR-3, we generated mice lacking a functional gene encoding VEGFR-3 by a knock-in strategy in which the bacterial  $\beta$ -galactosidase gene (*LacZ*) was placed in the first coding exon under the

control of the transcriptional regulatory sequences of VEGFR-3, deleting the beginning of the protein-coding region (Fig. 1) (10). The  $\beta$ -galactosidase ( $\beta$ -Gal) marker allows analysis of the pattern of VEGFR-3 gene expression in the gene-targeted mice.

Heterozygous mice and embryos appeared phenotypically normal, and the  $\beta$ -Gal expression in their tissues was consistent with that observed in VEGFR-3 in situ hybridization analysis of tissue sections (9). For example, large pericardial lymphatic vessels were detected in whole-mount staining of the heart of a newborn VEGFR-3<sup>+/-</sup> mouse (Fig. 2A), whereas only blood vessels were stained in a similar analysis of Tie-1<sup>+/-</sup> mice (11), which express  $\beta$ -Gal in endothelial cells (12). The stained vessels did not contain erythrocytes in sections of newborn skin, confirming their lymphatic nature (Fig. 2B). Also in E14.5 embryos, the developing lymphatic network of the skin was strongly stained, for example, around the developing ear (Fig. 2C). At E13.0, the expression was most prominent in venous sacs in the jugular and mesonephric regions and their surrounding vessels, supporting Sabin's theory on the origin of the first lymphatic vessels (13) (Fig. 2D).

To date, no live-born VEGFR-3<sup>-/-</sup> mice have been found. To determine the onset of embryonic lethality, we isolated embryos at

D. J. Dumont, Ontario Cancer Institute and Amgen Institute, Department of Medical Biophysics, University of Toronto, Toronto, Ontario, Canada M5G 2C1. L. Jussila, J. Taipale, A. Lymboussaki, T. Mustonen, K. Pajusola, K. Alitalo, Molecular/Cancer Biology Laboratory, Haartman Institute, University of Helsinki, PL 21 (Haartmaninkatu 3), 00014 Helsinki, Finland. M. Breitman, Samuel Lunenfeld Research Institute, Mount Sinai Hospital, Toronto, Ontario M5G 1X5, Canada.

\*These authors contributed equally to this work.

†Present address: Sunnybrook Health Science Centre, Division of Cancer Biology, S Wing Research Building, 2075 Bayview Avenue, Toronto, Ontario, M4N 3M5, Canada. ‡Deceased. §To whom correspondence should be addressed. E-mail: Kari.Alitalo@Helsinki.FI

## REPORTS

various stages of gestation. Homozygous VEGFR-3<sup>-/-</sup> embryos at E12.5 were severely necrotic (Table 1). At E10, the VEGFR-3<sup>-/-</sup> embryos were alive and could be identified by their underdeveloped yolk sac vasculature, which was pale and lacked major blood vessels (Fig. 3A), apparently because of a failure of remodeling of the yolk sac capillary network into complex vitelline vessels.

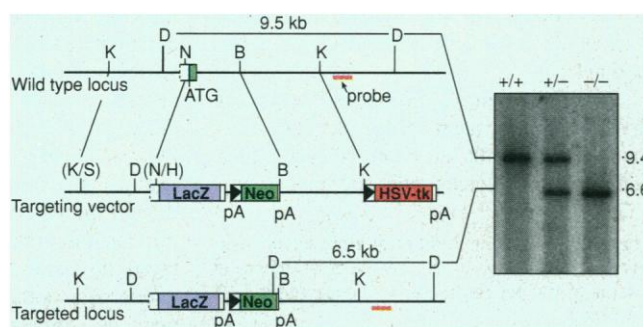
Whole-mount  $\beta$ -Gal staining analysis of

homozygous E9.5 VEGFR-3<sup>-/-</sup> embryos revealed an intense staining of an immature pattern of uniformly sized vessels in the developing head region making up the perineural vascular plexus (black arrow in Fig. 3B) (14). In contrast, in heterozygous embryos, VEGFR-3 expression was decreased in the mature perineural vessels (arrow in Fig. 3C). These results suggest that VEGFR-3 is necessary for the remodeling and maturation of

the perineural vascular plexus into a treelike hierarchy of large and small vessels and that its expression is subsequently decreased in the more mature vessels (15). In contrast, formation of new vessels by sprouting from preexisting ones, sprouting angiogenesis, apparently occurred in VEGFR-3<sup>-/-</sup> embryos, as evidenced by the presence of intersomitic vessels (arrowheads in Fig. 3, B and C). The pericardial cavity of the homozygous mutant embryos contained fluid or occasionally blood (red arrows in Fig. 3, B and D). In cross sections, the  $\beta$ -Gal staining was observed in endothelial cells of all developing blood vessels (Fig. 3E). In addition, the presence of erythrocytes in the VEGFR-3<sup>-/-</sup> embryos indicated that VEGFR-3 function is not necessary for primitive hematopoiesis.

Histological analysis of transverse sections of E10 VEGFR-3<sup>-/-</sup> embryos stained for the panendothelial marker, platelet-endothelial cell adhesion molecule-1 (PECAM-1) (16), showed that the embryos were severely growth retarded and the vasculature was underdeveloped when compared with heterozygous or wild-type embryos (Fig. 3, F and G).

**Fig. 1.** Gene targeting of the murine VEGFR-3 locus. The homologous recombination event deletes sequences encoding the initiation codon and signal peptide of the VEGFR-3 gene and places the LacZ gene under the control of the VEGFR-3 promoter and enhancer elements. Schematic structures of the wild-type and recombinant loci and the targeting vector are shown. K, Kpn I; B, Bam HI; S, Sal I; H, Hind III; N, Not I; D, Dra I; and pA, polyadenylation sequence.



(Inset) Southern blot analysis of E10.0 embryos after Dra I digestion with the indicated fragment (red bar) as the hybridization probe. Migration of DNA size markers (in kilobases) is shown on the right.

**Fig. 2 (top).** Whole-mount  $\beta$ -Gal staining of VEGFR-3 heterozygous embryos and tissues. (A) The heart of a newborn VEGFR-3<sup>+/-</sup> mouse reveals large lymphatic vessels (blue) at the pericardial surface. In contrast, coronary blood vessels (arrowheads) are not stained. (B) A section of newborn skin illustrating blue-stained lymphatic vessels (black arrowheads) and an unstained blood vessel containing erythrocytes (red arrowhead). E, epidermis. (C) Developing lymphatic network in the skin around the ear (asterisk) at E14.5. (D) At E13.0,  $\beta$ -Gal expression is most prominent at sites of lymphatic vessel development in the jugular (arrow) and perimesonephric (arrowhead) regions. Scale bars, 250  $\mu$ m.

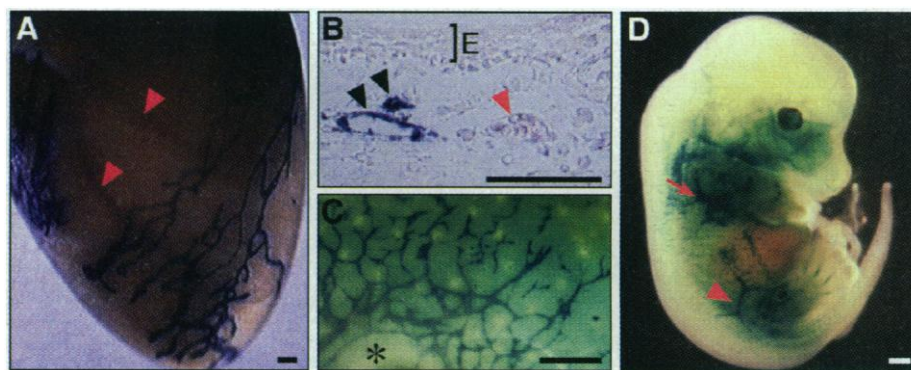
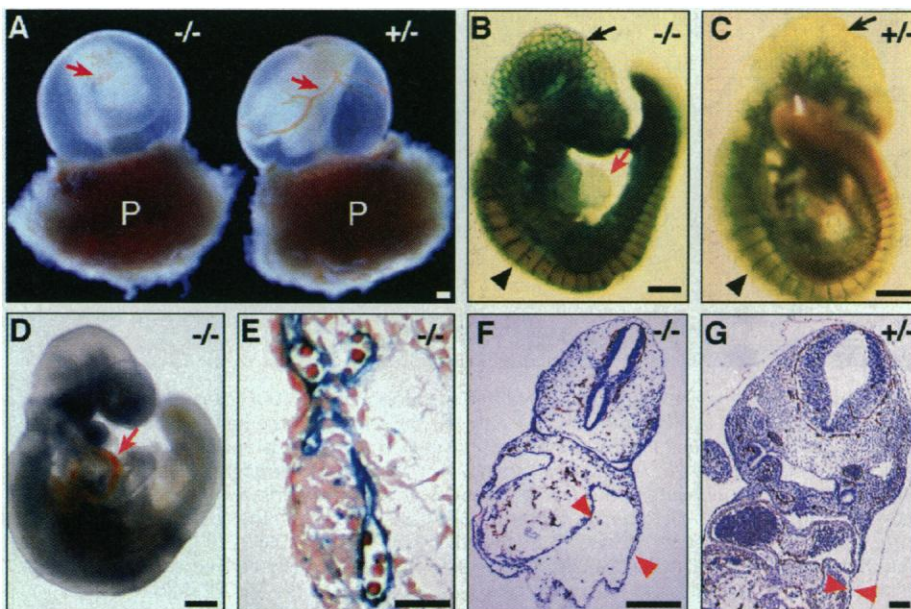


**Fig. 3 (bottom).** Whole-mount and histological analysis of VEGFR-3<sup>+/-</sup> and VEGFR-3<sup>-/-</sup> embryos. (A) Embryos at E10 were dissected from the uterus, and the decidua was removed to expose embryos with the yolk sac intact. The VEGFR-3<sup>-/-</sup> embryo (left) is identified by its underdeveloped yolk sac vasculature (arrows). P, placenta. Whole-mount  $\beta$ -Gal staining of E9.5 VEGFR-3<sup>-/-</sup> (B) and VEGFR-3<sup>+/-</sup> (C) embryos indicates that the pericardial cavity is enlarged (red arrow) and an immature perineural vascular plexus persists in the homozygote, whereas, in the heterozygote, vascular remodeling with down-regulation of  $\beta$ -Gal expression has occurred (black arrows). Intersomitic vessels appear similar in both cases (arrowheads). (D) Occasionally, blood was observed in the pericardial cavity of homozygous embryos. (E) A transverse section from the embryo in (B) reveals that the  $\beta$ -Gal-stained structures contain erythrocytes and thus are blood vessels. (F) At E10.0, the PECAM-1-stained VEGFR-3<sup>-/-</sup> embryo is growth retarded, the endothelial cells are fewer and disorganized, and the major vessels have not developed. (G) PECAM-1-stained VEGFR-3<sup>+/-</sup> embryo at E10. Note the differences in the sizes of the pericardial space [red arrowheads in (F) and (G)]. Scale bars: for (A) to (D), (F), and (G), 100  $\mu$ m; for (E), 50  $\mu$ m.



## REPORTS

At E9.0, whole-mount homozygous mutant embryos appeared indistinguishable from wild-type and heterozygous embryos. The myocardium, endocardium (11), and small vessels appeared normal in PECAM-1 staining of tissue sections (Fig. 4, A and B). In contrast, the staining revealed irregularly formed large vessels with defective lumens, including the anterior cardinal vein and dorsal aorta (arrows and arrowheads in Fig. 4, A and B, respectively).

The defects in the VEGFR-3<sup>-/-</sup> embryos were localized at putative sites of VEGFR-3 ligand signaling. For example, the VEGFR-3 gene was expressed at E9.0 in endothelial cells of the dorsal aorta (Fig. 4C) (17), and its ligand, VEGF-C, was expressed in the adjacent tissue (Fig. 4D). The yolk sac blood islands of the

homozygous and heterozygous knockout embryos were normal in structure, their endothelial cells expressed VEGFR-3 as determined by LacZ staining (Fig. 4, E and F) (17), and the mesodermal component also contained VEGF-C mRNA (Fig. 4, G and H). No VEGFR-3 RNA was detected in in situ hybridization analysis of sections from the VEGFR-3<sup>-/-</sup> embryos, confirming that the gene-targeting strategy had produced a null allele (Fig. 4, I to K). In contrast, the localization and intensity of the VEGF-C in situ hybridization signal were similar regardless of the VEGFR-3 genotype (11).

The embryonic cardiovascular system is the first organ system to develop (18). Formation of the yolk sac blood islands, which contain hematopoietic and endothelial pre-

cursors, and their subsequent remodeling into a functional circulatory system become critical for fetal survival beyond E9.5. The cardiovascular system is sensitive to perturbation, and its development is disrupted by a considerable number of mutations generated by homologous recombination (18). Embryos heterozygous for VEGF fail to develop major vessels and die at E11 to E12 (1). VEGFR-2-null embryos die at E8.5 to E9.5 because of an early defect in the development of hematopoietic and endothelial cells (2). Embryos deficient in VEGFR-1 show disorganized assembly of endothelial cells into functional vessels and die also at E8.5 to E9.5 (3), although mice lacking only the VEGFR-1 tyrosine kinase domain are viable (19). In contrast, the present results suggest that although the vascular remodeling and maturation are abnormal in the VEGFR-3-null embryos, no major defects occur in the differentiation of endothelial cells and in the formation of primary vascular networks by vasculogenesis or intersomitic vessels by endothelial cell sprouting. These differences in the null phenotypes strongly suggest that VEGFR-3 functions in a signaling pathway distinct from that used by the other VEGFRs.

Vascular remodeling defects and pericardial fluid accumulation similar to those described here have also been reported in embryos mutant for the transcription factors Scl/Tal (20), Tel-1 (21), and the tissue factor gene (22), but it is not known whether these genes act upstream or downstream of VEGFR-3. Other targeted mouse mutants with altered vascular development show increased endothelial cell apoptosis (23) or defects in endothelial cell sprouting (12, 24), signaling between arteries and veins in capillary morphogenesis (25), vessel stabilization (26, 27), pericyte migration (28), and tunica media formation (29).

The lymphangiogenic effects of VEGF-C (6) and its paracrine expression pattern with VEGFR-3 (9) have suggested that this ligand receptor pair functions in the developing and adult lymphatic system. Our present results provide evidence that VEGFR-3 is important for the remodeling and maturation of primary vascular networks into larger blood vessels and that the VEGFR-3 signaling pathway is necessary for the early development of the cardiovascular system.

**Table 1.** VEGFR-3 genotypes and corresponding phenotypes. Data are the number of embryos or mice with the indicated genotype from VEGFR-3<sup>+/-</sup> breeding pairs. After E9, all the VEGFR-3<sup>-/-</sup> embryos were growth retarded; they were necrotic after E12.5. Edema of the pericardial sac was observed at E10 in 82% (9 out of 11) of the null embryos. ND, not determined.

Age	VEGFR-3 <sup>+/+</sup>	VEGFR-3 <sup>+/-</sup>	VEGFR-3 <sup>-/-</sup>	ND	Total
E9.0 to E9.5	31	51	19	13	114
E10.0	19	24*	11	1	55
E12 to E13	9	19	3†	6	37
E14	4	6	2†	4	16
Adults	53	83	0	0	136

\*A single E10 VEGFR-3<sup>+/-</sup> embryo had edema of the pericardium. †Necrotic.

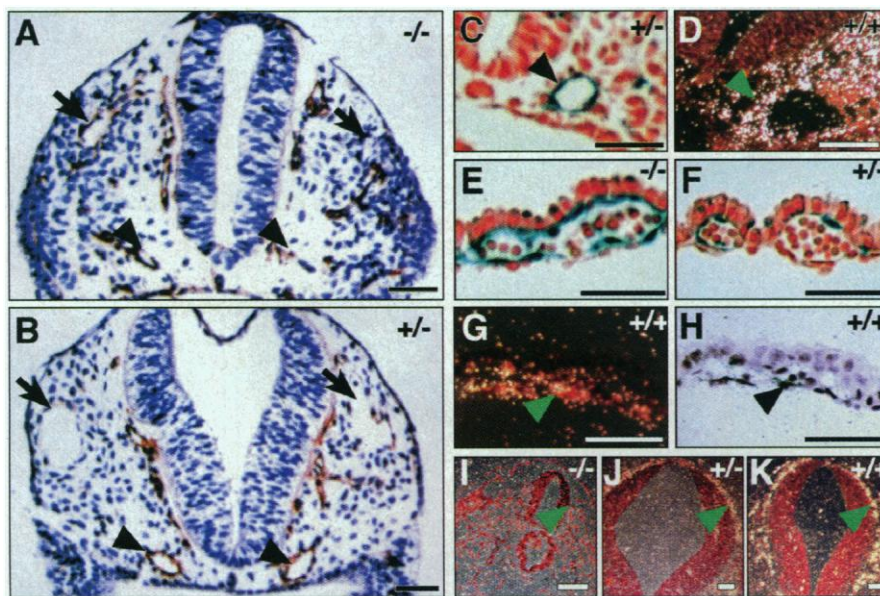


**Fig. 4.** Immunohistochemical and in situ hybridization analysis of the VEGFR-3-null embryos. Blood vessels were identified by PECAM-1 staining; only the region around the neural tube is shown for clarity. At E9.0, the vasculature of the homozygous null embryo (A) is underdeveloped, and the major vessels, the weakly PECAM-stained cardinal vein (arrow), and strongly stained dorsal aorta (arrowhead) appear rudimentary; their lumens are defective in comparison with the heterozygous embryos in (B). At E9.0,  $\beta$ -Gal staining indicates VEGFR-3 expression in the endothelial cells of the dorsal aorta (C) and yolk sac (E and F) of the VEGFR-3<sup>-/-</sup> and VEGFR-3<sup>+/-</sup> embryos. In situ hybridization analysis shows that VEGF-C is expressed in mesodermally derived cells of the aortal region (D) and of the yolk sac [(G), dark field; (H), bright field]. No VEGFR-3 RNA signal was obtained from sections of VEGFR-3<sup>-/-</sup> embryos (I), whereas weak and strong signals were detected in blood vessels surrounding the neural tube (arrowheads) from heterozygous (J) and wild-type (K) embryos, respectively. Scale bars, 75  $\mu$ m.

### References and Notes

1. P. Carmeliet et al., *Nature* **380**, 435 (1996); N. Ferrara et al., *ibid.*, p. 439.
2. F. Shalaby et al., *ibid.* **376**, 62 (1995).
3. G. H. Fong, J. Rossant, M. Gertsenstein, M. L. Breitman, *ibid.*, p. 66.
4. N. Ferrara and T. Davis-Smyth, *Endocr. Rev.* **18**, 4 (1997); E. I. Korpelainen and K. Alitalo, *Curr. Opin. Cell Biol.* **10**, 159 (1998).
5. J. E. Park et al., *J. Biol. Chem.* **269**, 25646 (1994); A. Sawano et al., *Cell Growth Differ.* **7**, 213 (1996); B. Olofsson et al., *Proc. Natl. Acad. Sci. U.S.A.* **95**, 11709 (1998).

6. M. Jeltsch *et al.*, *Science* **276**, 1423 (1997); S. J. Oh *et al.*, *Dev. Biol.* **188**, 96 (1997).
7. V. Joukov *et al.*, *EMBO J.* **15**, 290 (1996); J. Lee *et al.*, *Proc. Natl. Acad. Sci. U.S.A.* **93**, 1988 (1996).
8. M. G. Achen *et al.*, *Proc. Natl. Acad. Sci. U.S.A.* **95**, 548 (1998); A. Eichmann *et al.*, *Development* **125**, 743 (1998).
9. A. Kaipainen *et al.*, *Proc. Natl. Acad. Sci. U.S.A.* **92**, 3566 (1995); E. Kukk *et al.*, *Development* **122**, 3829 (1996).
10. We generated a null VEGFR-3 allele by introducing a LacZ cassette into the VEGFR-3 locus (71). The 3-kb Kpn I–Not I and Bam HI–Kpn I fragments from 129SV mouse genomic DNA library ( $\lambda$ FIX II; Stratagene) were used as the arms of the targeting vector (Fig. 1). The gene-targeting event was confirmed by Southern (DNA) blot analysis (Fig. 1) (D. J. Dumont *et al.*, data not shown), and two independent embryonic stem cell lines were used to make heterozygous mice through blastocyst injection. Wild-type, heterozygous, and homozygous embryos and mice were identified by Southern blot analysis of yolk sac and tail DNA, respectively.
11. L. Jussila, J. Taipale, K. Alitalo, unpublished data.
12. M. C. Puri *et al.*, *EMBO J.* **14**, 5884 (1995).
13. F. R. Sabin, *Anat. Rec.* **6**, 335 (1912).
14. Embryos were stained for  $\beta$ -Gal (12), photographed, and subsequently dehydrated and embedded in paraffin. Seven-micrometer sections were stained immunohistochemically for PECAM-1 (Pharmingen, San Diego, CA) with TSA Kit (NEN, Boston, MA). Mouse VEGFR-3 [base pairs (bp) 22 to 214; GenBank U7296] and VEGF-C (bp 499 to 656; GenBank U73620) cDNA probes were used for in situ hybridization (9).
15. For a review, see W. Risau, *Nature* **386**, 671 (1997).
16. A. Vecchi *et al.*, *Eur. J. Cell Biol.* **63**, 247 (1994).
17. The presence of VEGFR-3 mRNA in endothelial cells of the dorsal aorta and the yolk sac was confirmed by in situ hybridization (A. Lybroussaki and K. Alitalo, data not shown).
18. J. Rossant, *Circ. Res.* **78**, 349 (1996).
19. S. Hiratsuka *et al.*, *Proc. Natl. Acad. Sci. U.S.A.* **95**, 9349 (1998).
20. J. E. Visvader, Y. Fujiwara, S. H. Orkin, *Genes Dev.* **12**, 473 (1998).
21. L. C. Wang *et al.*, *EMBO J.* **16**, 4374 (1997).
22. P. Carmeliet *et al.*, *Nature* **383**, 73 (1996).
23. L. Wojnowski *et al.*, *Nature Genet.* **16**, 293 (1997).
24. T. N. Sato *et al.*, *Nature* **376**, 70 (1995).
25. H. U. Wang, F.-F. Chen, D. J. Anderson, *Cell* **93**, 741 (1998).
26. M. Oshima, H. Oshima, M. M. Taketo, *Dev. Biol.* **179**, 297 (1996).
27. C. Suri *et al.*, *Cell* **87**, 1161 (1997).
28. P. Lindahl *et al.*, *Science* **277**, 242 (1997).
29. C. T. K. Kuo *et al.*, *Genes Dev.* **11**, 2996 (1997).
30. We thank A. Kaipainen for helpful discussions, E. Koivunen for expert help with the mice, and M. Helanterä, P. Ylikantola, and T. Tainola for technical assistance. Supported by research grants from the Medical Research Council (Canada) and AMGEN (to D.J.D.) and by the Finnish Cancer Organizations, the Finnish Academy, the Sigrid Juselius Foundation, the Finnish State Technology Development Centre, and the European Union Biomed Program.

15 July 1998; accepted 30 September 1998

## Loss of Intraspecific Aggression in the Success of a Widespread Invasive Social Insect

David A. Holway,\* Andrew V. Suarez, Ted J. Case

Despite the innumerable ecological problems and large economic costs associated with biological invasions, the proximate causes of invasion success are often poorly understood. Here, evidence is provided that reduced intraspecific aggression and the concomitant abandonment of territorial behavior unique to introduced populations of the Argentine ant contribute to the elevated population densities directly responsible for its widespread success as an invader. In the laboratory, nonaggressive pairs of colonies experienced lower mortality and greater foraging activity relative to aggressive pairs. These differences translated into higher rates of resource retrieval, greater brood production, and larger worker populations.

Biological invasions threaten the integrity of the world's biota (1, 2). Of the many invading organisms, social insects are among the most harmful: their invasions damage agricultural systems, disrupt natural communities, affect large geographic areas, and are expensive to control (3). Here, we used an experimental approach to investigate the mechanisms underlying the success of a widespread invasive social insect, the Argentine ant (*Linepithema humile*). Experimental approaches are essential to understanding the basis of invasion success (4), but such studies are rare (5).

Ant colonies often have well-defined territorial boundaries, a condition referred to as multicoloniality (6). Multicolonial ants defend their territories aggressively, particularly against conspecifics. Such behavior is thought to limit population density in ants (6, 7), and for animals generally (8), because

territorial defense expends resources, time, and energy that could otherwise be allocated to growth, maintenance, and reproduction (9). Not all ants defend territories. In unicolonial species, for example, intraspecific aggression is reduced, colony boundaries are weak to nonexistent, and supercolonies composed of interconnected nests are the norm (6, 7). Worker populations of unicolonial ants often attain high densities (7, 10, 11), perhaps because unicolonial species are exempt from the costs of defending territories against conspecifics. Numerical advantages, stemming from high population densities, are key to the competitive ability of many ants (12, 13), including invasive species (10, 14).

Native to South America, the Argentine ant has been introduced into areas with Mediterranean and subtropical climates throughout the world, where it displaces native ants (6, 11, 15) and other arthropods (16) and disrupts mutualisms (17). In its introduced range, *L. humile* is highly unicolonial, occupying expansive supercolonies that lack clear behavioral borders (6, 18, 19). In southern

California, for example, intraspecific aggression is rare, even over large spatial scales (>100 km), suggesting the presence of expansive supercolonies (19). In its native range, Argentine ants exhibit pronounced intraspecific aggression over small spatial scales (<100 m) and maintain colony structures more closely resembling those of multicolonial ants (19). This variation in the occurrence of intraspecific aggression among colonies permits a direct test of the mechanisms responsible for the elevated population densities typical of unicolonial ants. Moreover, this variation provides an unparalleled opportunity to assess experimentally how territoriality may limit population size (20).

We tested the relationship between intraspecific aggression and population size by rearing pairs of lab colonies that either did or did not exhibit intraspecific aggression. To do this, we sampled workers and queens from spatially separate nests in southern California (21). We then set up 44 experimental colonies (22), each consisting of three queens, 500 workers, and <50 brood pieces. Using plastic tubing, we connected colonies into pairs via a common foraging arena. Colony pairs were placed into three experimental categories on the basis of the origin of each nest and whether they exhibited intraspecific aggression (23). Categories included an aggressive treatment (pairs that exhibited aggression and were collected from different sites), a nonaggressive treatment (pairs that did not exhibit aggression and were collected from different sites), and a control (colonies from the same site). For each colony pair, we quantified intraspecific aggression (24), worker mortality, foraging activity, resource retrieval rates, and productivity (25).

Throughout the experiment, workers from the aggressive treatment group remained aggressive (often fighting to the death), whereas workers from the nonaggressive treatment and control groups rarely showed any sign of

Department of Biology, University of California, San Diego, 9500 Gilman Drive, La Jolla, CA 92093, USA.

\*To whom correspondence should be addressed. E-mail: dholway@biomail.ucsd.edu